Available online at www.sciencedirect.com
ScienceDirect
Journal of Sound and Vibration 322 (2009) 358–380
JOURNAL OF SOUND AND VIBRATION
www.elsevier.com/locate/jsvi

Non-resonant double Hopf bifurcations: The complex case

Griselda R. Itovich[a], Jorge L. Moiola[b,*]

[a]*Departamento de Matemática, FaEA, Universidad Nacional del Comahue, Buenos Aires 1400, (8300) Neuquén, Argentina*
[b]*Instituto de Investigaciones en Ingeniería Eléctrica-IIIE (UNS-CONICET), Departamento de Ingeniería Eléctrica y de Computadoras, Universidad Nacional del Sur, Avenida Alem 1253, (8000) Bahía Blanca, Argentina*

Received 6 March 2008; received in revised form 26 August 2008; accepted 7 November 2008
Handling Editor: S. Bolton
Available online 20 December 2008

Abstract

The analysis of the unfolding of a non-resonant double Hopf singularity is considered using the frequency domain and the normal form methodologies. A higher-order harmonic balance and the evaluation of Floquet multipliers are used to obtain accurate approximations of the limit cycles and its local bifurcations. This type of hybrid methodology using harmonic balance and normal forms gives a complementary view in the vicinity of the singularity. More specifically, some of the bifurcation curves arising in the unfolding of the double Hopf bifurcation are computed with great accuracy using the harmonic balance method compared to the classical normal form. However, this last method is able to predict the appearance of complex quasiperiodic behavior such as three-dimensional (3D) torus. Numerical simulations corroborate this observation.

0. Introduction

Hopf bifurcation degeneracies can be divided into two distinctive groups: (a) Those that can be treated properly through singularity theory [1] which involve the so-called transversality crossing failure and/or the vanishing of the stability index and (b) those related on multiple crossings of eigenvalues through the imaginary axis. Within the last group, the non-resonant double Hopf (DH) and the Gavrilov–Guckenheimer (also called zero-Hopf or fold-Hopf) singularities are some of the most studied [2]. The local dynamic analysis of these two codimension degeneracies can be carried out applying normal forms theory, methodology that nowadays results available thanks to the implementation of certain routines under the most popular computer algebra software [3,4]. Both singularities are always related with the existence of quasiperiodic solutions or two-dimensional (2D) tori emerging from Neimark–Sacker bifurcation curves. Oftentimes, cyclic fold bifurcations are also detected close to DH bifurcations [5], whereas period-doubling ones are usual when the case fold-Hopf is treated [6]. For the last case, see also a more detailed analysis in the unfolding of a triple zero degeneracy in Ref. [7].

*Corresponding author.
E-mail addresses: gitovich@arnet.com.ar (G.R. Itovich), jmoiola@criba.edu.ar (J.L. Moiola).

0022-460X/$ - see front matter © 2008 Elsevier Ltd. All rights reserved.
doi:10.1016/j.jsv.2008.11.005

Specifically, when the non-resonant DH singularity is considered under normal forms [2] two cases can be clearly distinguished: the simple case, which leads to the strict appearance of toroidal solutions, and the difficult or complex case. The last situation can be related occasionally with the bifurcations of the aforementioned quasiperiodic solutions, which give the presence of a new orbit composed by three oscillatory modes (3D torus). In this framework, another criterion to analyze the local dynamics of the DH bifurcation can be adapted from the frequency domain approach [8,9]. These techniques allow to build the Hopf bifurcation curve which crosses the singularity precisely as well as the branches of Neimark–Sacker bifurcations that emerge from there [5]. Thus, several regions with characteristic dynamic behavior assemble the unfolding of the DH singularity. Following these ideas, the analysis of other Hopf degeneracies has also been developed satisfactorily [10]. Furthermore, other interesting contributions of the frequency domain-like approach appear when the goal is focused on handling static [11], dynamic [12,13] or period-doubling bifurcations [14] for bifurcation control purposes.

When the non-resonant DH singularity arises it is inevitable to think that it comes from a model of coupled oscillators. This idea has been used to analyze electrical circuits [15], a combination of electrical and mechanical models [16], chemical reactions systems [17], mechanical devices [18,19] and problems in fluid dynamics [20,21]. In all the mentioned situations, the presence of quasiperiodic solutions is detected employing normal forms or by a discrete treatment through the Poincaré map. Particularly, in Refs. [19,22] a type of complex case of the singularity is shown, when bifurcations of quasiperiodic solutions appear and lead to 3D tori. Moreover, if this situation repeats over and over, a sequence of Neimark–Sacker bifurcations can lead to chaos, as it appears to be the preferred route in high-dimensional systems [23]. Finally, it is also important to mention that a quite analogous phenomenon of DH bifurcation for maps has been analyzed very recently in vibratory systems with rigid stops subjected to periodic excitation [24] (see also Ref. [25] for the creation of the bifurcation via feedback control).

This work is organized as follows. In Section 2 a summary to analyze Hopf bifurcations in the frequency domain is stated. The stability of the emergent cycles as well as its possible bifurcations is considered in Section 3. Later, an introduction of the general treatment of the non-resonant DH singularity under normal forms is included in Section 4, where it is also specified the dynamics in the neighborhood of the singularity. In Section 5, an example derived from a coupled electrical circuit is analyzed in detail through the frequency domain methodology and normal forms theory. In this model, it is recognized the dynamics of a DH singularity which gives place to the existence of 3D torus. Moreover, all standard local cyclic bifurcations are detected close to criticality: from Neimark–Sacker curves which are originated at DH bifurcation, up to fold and period-doubling bifurcations which are not standard in the bifurcation diagrams in the unfolding of this singularity [2]. In this intricate scenario, other Hopf degeneracies and complex singularities (specially a Gavrilov–Guckenheimer bifurcation) appear and generate new quasiperiodic solutions besides the presence of strange attractors. At last, the conclusions are presented in Section 6.

1. Frequency domain methodology

The starting point is a nonlinear system like

$$\dot{x} = f(x;\eta), \quad x(0) = 0, \tag{1}$$

where $\dot{x} = \mathrm{d}x/\mathrm{d}t$, $x \in R^n$, $\eta \in R^l$. The variable x depicts a state vector of Eq. (1) which depends on the time t, and η identifies a bifurcation parameter vector of the problem. This approach is based on the fact that Eq. (1) can be written also as

$$\dot{x} = Ax + B(Dy + u), \quad y = Cx, \tag{2}$$

$$u = g(e;\eta) = \tilde{g}(y;\eta) - Dy, \tag{3}$$

where $y \in R^m$ is the so-called output variable, $u \in R^p$ can be viewed as control input, A, B, C and D of orders $n \times n$, $n \times p$, $m \times n$ and $p \times m$, respectively, and they may depend on η. Moreover, the matrix A is supposed non-singular for any choice of η, the function $\tilde{g} : R^m \times R^l \longrightarrow R^p$, comes through the selected matrices and the function f, where $e = -y$, and it is considered that both $\tilde{g}$, $g \in C^{2r+1}$, $r \geqslant 4$. The analysis in the frequency

domain is achieved by applying the Laplace transform to Eqs. (2) and (3) with the condition $x(0)=0$, and solving the equilibrium equation

$$e = -G(0;\eta)g(e;\eta), \tag{4}$$

where $G(s;\eta) = C(\eta)[s * I - (A(\eta) + B(\eta)D(\eta)C(\eta))]^{-1}B(\eta)$ is the usual transfer matrix of the linear part of Eq. (2). The solution of Eq. (4) is in correspondence with the equilibrium of the original system satisfying $f(x;\eta)=0$. Let $\tilde{x}$ and $\tilde{e}$ be the names of a certain equilibrium in time (Eq. (1)) and in the frequency (Eq. (4)) domains, respectively. In time domain, the character of an equilibrium point is analyzed via the Jacobian matrix of the system and thus, when one single eigenvalue (or a pair of complex eigenvalues) crosses the imaginary axis, then a bifurcation of equilibrium is expected to appear. Defining the $p \times m$ matrix

$$J(\eta) = D_1 g(e;\eta)|_{e=\tilde{e}} = \left[\left.\frac{\partial g_j}{\partial e_k}\right|_{e=\tilde{e}}\right], \tag{5}$$

the following result in the frequency domain can be stated.

Lemma 1. *If the linearization of Eq.* (1) *evaluated at the equilibrium* $\tilde{x}$ *has an imaginary pure eigenvalue* $\mathrm{i}\omega_0$ *for* $\eta=\eta_0$ *then its image eigenvalue of the matrix* $GJ = G(s;\eta)J(\eta)$ *evaluated at* $\tilde{e}$ *passes through* $(-1+\mathrm{i}0)$ *in the complex plane, when* $s=\mathrm{i}\omega_0$ *and* $\eta=\eta_0$.

Proof. Using the generalized Nyquist stability criterion, the authors in Ref. [8] showed this result. □

Thereby, the bifurcation analysis can be understood as a graphical problem in the complex plane. Carrying on with this approach and aiming to set the corresponding Hopf bifurcation theorem, it is considered the characteristic polynomial of the matrix GJ, namely

$$h = h(\lambda, s;\eta) = \det(\lambda * I - G(s;\eta)J(\eta)). \tag{6}$$

Due to the last lemma, two associated functions are defined by separating the real and imaginary parts of the previous expression

$$F_1(\omega,\eta) = \mathrm{Re}(h(-1,\mathrm{i}\omega;\eta)), \tag{7}$$

$$F_2(\omega,\eta) = \mathrm{Im}(h(-1,\mathrm{i}\omega;\eta)). \tag{8}$$

The functions F_1 and F_2 can be used to formulate necessary conditions to guarantee the existence of static and dynamic (or Hopf) bifurcations as well as its degeneracies [9,10]. Following this framework and now with $\eta \in R$, the Hopf bifurcation theorem is established:

Theorem 1. *Consider Eq.* (1) *written as Eqs.* (2) *and* (3).

It is supposed that the three following hypotheses are fulfilled:

(H1) *There is only one solution* $\hat{\lambda}$ (*eigenvalue of the matrix GJ*) *for the equation* $h(\lambda,\mathrm{i}\omega;\eta)=0$, *which crosses* $(-1+\mathrm{i}0)$ *for a certain value* $\omega=\omega_0\neq 0$ (*unique too*) *when* $\eta=\eta_0$ *and it is related with a stability change of the equilibrium* $\tilde{e}$. *Furthermore*, $\partial F_1/\partial\omega|_{(\omega_0,\eta_0)}$, $\partial F_2/\partial\omega|_{(\omega_0,\eta_0)}$ *do not vanish simultaneously, where* F_1 *and* F_2 *have been defined in Eqs.* (7) *and* (8).

(H2) *The determinant*

$$M_1 = \left|\left.\frac{\partial(F_1,F_2)}{\partial(\omega,\eta)}\right|_{(\omega_0,\eta_0)}\right| = \left|\begin{array}{cc} \dfrac{\partial F_1}{\partial\omega} & \dfrac{\partial F_1}{\partial\eta} \\ \dfrac{\partial F_2}{\partial\omega} & \dfrac{\partial F_2}{\partial\eta} \end{array}\right|_{(\omega_0,\eta_0)} \tag{9}$$

is non-zero.

(H3) *The curvature coefficient* (*also known as the first Lyapunov coefficient*) *defined as*

$$\sigma_1 = -\mathrm{Re}\left(\frac{u^{\mathrm{T}}G(\mathrm{i}\omega_0;\eta_0)p_1(\omega_0,\eta_0)}{u^{\mathrm{T}}G'(\mathrm{i}\omega_0;\eta_0)J(\eta_0)v}\right) \tag{10}$$

has sign definition.

Under the above conditions, Eq. (1) has one branch of periodic solutions which starts at $\eta = \eta_0$, and its direction and stability depend on the signs of M_1 and σ_1.

Proof. See Ref. [8].

Observation: In Eq. (10), u^{T} and v are the normalized left and right eigenvectors of the matrix $G(\mathrm{i}\omega_0;\eta_0)J(\eta_0)$ associated with the eigenvalue $\hat{\lambda}$ ($\bar{u}^{\mathrm{T}}v = 1$ and $\bar{v}^{\mathrm{T}}v = 1$, where "—" means complex conjugation), $G' = \mathrm{d}G/\mathrm{d}s$ and p_1 is a p-dimensional vector with complex components

$$p_1(\omega,\eta) = QV_{02} + \tfrac{1}{2}\overline{Q}V_{22} + \tfrac{1}{8}L\bar{v}, \tag{11}$$

whose computation requires the second and third derivatives of the function g [8] through the calculation of the matrices Q, $\overline{Q}$ and L of order $p \times m$, defined as

$$Q = Q(\eta) = D_2 g(e;\eta)|_{e=\tilde{e}} = \left[\sum_{l=1}^{m} \frac{\partial^2 g_j}{\partial e_l \partial e_k}\bigg|_{\tilde{e}} v_l\right], \tag{12}$$

where $v = [v_1 \;\; v_2 \;\; \cdots \;\; v_m]^{\mathrm{T}}$,

$$\overline{Q} = \overline{Q}(\eta) = \left[\overline{\sum_{l=1}^{m} \frac{\partial^2 g_j}{\partial e_l \partial e_k}\bigg|_{\tilde{e}} v_l}\right] = \left[\sum_{l=1}^{m} \frac{\partial^2 g_j}{\partial e_l \partial e_k}\bigg|_{\tilde{e}} \overline{v_l}\right], \tag{13}$$

and

$$L = L(\eta) = D_3 g(e;\eta)|_{e=\tilde{e}} = \left[\sum_{l=1}^{m}\sum_{i=1}^{m} \frac{\partial^3 g_j}{\partial e_l \partial e_i \partial e_k}\bigg|_{\tilde{e}} v_l v_i\right], \tag{14}$$

where $j = 1,2,\ldots,p$; $k = 1,2,\ldots,m$. Besides, the following vectors are defined:

$$V_{02} = -\tfrac{1}{4}H(0;\eta)Q\bar{v}, \tag{15}$$

$$V_{11} = v, \tag{16}$$

$$V_{22} = -\tfrac{1}{4}H(\mathrm{i}2\omega;\eta)Qv, \tag{17}$$

where $H(s;\eta) = [I + G(s;\eta)J(\eta)]^{-1}G(s;\eta)$ is the closed-loop transfer matrix for the feedback system which comes from Eqs. (2) and (3). All the computed vectors are the result of a second-order harmonic balance between the linear transfer matrix $G(s;\eta)$ and the nonlinear feedback path $g(e;\eta)$. □

Theorem 1 is also known as graphical Hopf theorem and it aims to prove the existence of a periodic solutions branch born at η_0. The technique is constructive and considers the intersection between two eigenlocus: one depicted by the eigenvalue $\hat{\lambda}$ and the other coming from an amplitude function $\mathscr{A}_1$. The former locus carries on the effect of the linearity of the so-called transfer matrix GJ while the latter summarizes the influence of the nonlinearity in the feedback path [8,26]. This procedure allows to estimate the frequency $\hat{\omega}$ and the amplitude $\hat{\theta}$ of the periodic solution which appears for $\tilde{\eta}$ close to η_0 and therefore to give a kind of quasianalytical approximate expression. Specifically, employing a second-order harmonic balance results

$$e = e(t;\tilde{\eta}) = \tilde{e}(\tilde{\eta}) + \mathrm{Re}\left(\sum_{k=0}^{2} E_k^2 \exp(\mathrm{i}k\hat{\omega}t)\right), \tag{18}$$

where

$$E_0^2 = V_{02}\hat{\theta}^2, \quad E_1^2 = V_{11}\hat{\theta} + V_{13}\hat{\theta}^3, \quad E_2^2 = V_{22}\hat{\theta}^2, \tag{19}$$

according to Eqs. (15)–(17), and the vector V_{13} can be computed as described in Ref. [26]. These results proceed from the most elemental formulation of the Hopf theorem in the frequency domain. Then a much more precise (although still local) orbit expression is obtained by considering higher-order harmonic balance solutions [9,26]. This kind of approximations (which are iterative) involves up to eight harmonics. This means to take care of the ninth-order derivative in the expansion of $g(e;\eta)$ about the equilibrium $\tilde{e}$. This higher

expansion will be the tool to detect limit cycle bifurcations. Moreover, one alternative of the described method is called the modified scheme [9]. It gives rather accurate results when the limit cycles grow substantially despite of perturbing slightly the main parameter. This scheme is also used specially when multiple (nested) limit cycles are involved.

2. Stability and bifurcations of periodic solutions

When a nonlinear system like given by Eq. (1) has a T-periodic solution $\mathbf{\Gamma}$, its stability can change and its consequences follow from the study of the return or Poincaré map P. So if $x_0 \in \mathbf{\Gamma}$ the linearization $D_1P(x_0)$ is an $(n-1)\times(n-1)$-matrix and if all the eigenvalues of $D_1P(x_0)$ are located inside the unit circle, then $\mathbf{\Gamma}$ is asymptotically stable. However, usually it is not possible to find an explicit expression for the map $P(x_0)$, which would simplify the computation of the eigenspectrum of $D_1P(x_0)$. Hence, it is considered the following system:

$$\dot{z} = S(t)z, \tag{20}$$

where

$$\dot{z} = \frac{\mathrm{d}z}{\mathrm{d}t}, \quad z \in R^n$$

and

$$S(t) = D_1 f(\mathbf{\Gamma}(t;\tilde{\eta});\tilde{\eta}) = \left.\frac{\partial f}{\partial x}\right|_{x=\mathbf{\Gamma}(t;\tilde{\eta}),\eta=\tilde{\eta}}, \quad S(t+T) = S(t),$$

where T is the period of the orbit $\mathbf{\Gamma}$.

Suppose one finds out a fundamental solution matrix of Eq. (20) $M = M(t)$ with initial conditions $M(0) = I$, where I is the identity matrix of order n. By computing $M(T)$, one obtains the so-called monodromy matrix of the orbit $\mathbf{\Gamma}$. Its n eigenvalues, known as characteristic or Floquet multipliers of the periodic solution $\mathbf{\Gamma}$, are $\mu_0 = 1$ and $\{\mu_i\}_{i=1}^{n-1}$, where $\{\mu_i\}_{i=1}^{n-1}$ are the eigenvalues of $D_1P(x_0)$. A bifurcation of the cycle Γ happens when one eigenvalue of $D_1P(x_0)$ is crossing the unit circle. If that eigenvalue is $\mu_1 = 1$, the map $P(x_0)$ may have a saddle-node (also called fold bifurcation), transcritical or pitchfork bifurcation, and the original system (1) exhibits none, one, two or more limit cycles on both sides of the bifurcation. If $\mu_1 = -1$, a period-doubling or flip bifurcation appears together with two periodic solutions: one normally has a switch on the stability and the new cycle shows a period which doubles the former's. Finally, if $D_1P(x_0)$ has a pair of complex conjugate eigenvalues on the unit circle, system (1) usually shows a quasiperiodic solution which almost describes the surface of a bidimensional or 2D torus. In this case, a Hopf or Neimark–Sacker bifurcation of the Poincaré map $P(x_0)$ is established.

3. Non-resonant DH bifurcation

If the linearization matrix of Eq. (1) evaluated at the equilibrium has a pair of imaginary pure eigenvalues but at least one of the hypotheses of Theorem 1 fails, a Hopf degeneracy appears. The cases where the hypotheses H2 or/and H3 are not satisfied have been studied through singularity theory with local techniques [1] in time domain, and with the same ideas some singularities have been analyzed in Ref. [9] with the frequency domain formalism. In this sense, the analysis of the emergent dynamics shows the appearance of multiple Hopf points, the simultaneous existence of multiple cycles or a combination of both. On the contrary, the situations where the hypothesis H1 fails deal with some global bifurcations, involving, generally, homoclinic or heteroclinic orbits and hence complex dynamics. This is the case of the singularity known as Gavrilov–Guckenheimer bifurcation (fold-Hopf and pitchfork-Hopf are other usual names), where the linearization of the system evaluated at the equilibrium has a zero and a pair of imaginary pure eigenvalues and the non-resonant DH bifurcation which appears when there are two pairs of eigenvalues $\pm i\omega_1$, $\pm i\omega_2$, $\omega_1/\omega_2 \in I$ (the resonant case is defined when the ratio of the frequencies is $k:1$, $k \in N$). Anyway, if one is interested in the bifurcations of each one of the limit cycles coming from Hopf curves, the higher-order

approximations, which can include up to eight harmonics, can be considered. Then, the monodromy matrix can be used to establish, at least locally, the appearance of quasiperiodic solutions via the mechanism of Neimark–Sacker bifurcations. The dynamics of the neighborhood of both singularities can be described through two independent parameters, which classify them as codimension two bifurcation points. Hence, the main objective is to analyze profoundly the local dynamics of a non-resonant DH point. For this reason, it is supposed that the system equilibrium is $\tilde{x}=0$ and its associated linearization has only four eigenvalues on the imaginary axis, as has been stated before. Thus, the classical analysis of a non-resonant DH bifurcation is based on the application of normal forms theory [27] which is summarized forthwith. Due to the aforementioned assumptions, it is sufficient to consider the system

$$\dot{x}=f(x;\eta), \tag{21}$$

where $x\in R^4$, $\eta=(\eta_1,\ \eta_2)\in R^2$. If $\eta=0$, the linearization of Eq. (21) about the equilibrium point has two pairs of eigenvalues $\pm i\omega_1$, $\pm i\omega_2$, $\omega_1/\omega_2\in I$, where $\omega_1>\omega_2>0$. Employing the method of multiple scales, a normal form with terms up to third order is achieved [4], which can be expressed in polar coordinates in the following way:

$$\dot{r}_1=r_1(\alpha_{11}\eta_1+\alpha_{12}\eta_2+p_{11}r_1^2+p_{12}r_2^2), \tag{22}$$

$$\dot{r}_2=r_2(\alpha_{21}\eta_1+\alpha_{22}\eta_2+p_{21}r_1^2+p_{22}r_2^2), \tag{23}$$

$$\dot{\phi}_1=\omega_1+\psi_1(r_1,r_2;\eta), \tag{24}$$

$$\dot{\phi}_2=\omega_2+\psi_2(r_1,r_2;\eta), \tag{25}$$

where α_{ij}, p_{ij}, $i,j=1,2$, are constants. The equilibrium points can be easily found now, solving $\dot{r}_1=\dot{r}_2=0$. Thus, one obtains:

(1) $E_0: r_1=0,\ r_2=0$, which is the trivial equilibrium point,
(2) $E_1: r_1^2=-\Omega_1/p_{11}$, $r_2=0$, where $\Omega_1=\alpha_{11}\eta_1+\alpha_{12}\eta_2$ and $p_{11}\neq 0$, which means a periodic solution due to a Hopf bifurcation, with frequency $\tilde{\omega}_1$ close to the critical frequency ω_1,
(3) $E_2: r_1=0$, $r_2^2=-\Omega_2/p_{22}$, where $\Omega_2=\alpha_{21}\eta_1+\alpha_{22}\eta_2$ and $p_{22}\neq 0$, which depicts a periodic solution due to a Hopf bifurcation, with frequency $\tilde{\omega}_2$ close to the critical frequency ω_2,
(4) $E_3: r_1^2=(p_{12}\Omega_2-p_{22}\Omega_1)/\Delta, r_2^2=(p_{21}\Omega_1-p_{11}\Omega_2)/\Delta$, where $\Delta=p_{11}p_{22}-p_{12}p_{21}\neq 0$, which represents a quasiperiodic solution or 2D torus with approximate frequencies $\tilde{\omega}_1$ and $\tilde{\omega}_2$, close to ω_1 and ω_2, respectively.

The normal form of Eqs. (22)–(25) is simpler than the one introduced by Kuznetsov [2], who includes fifth-order terms and bases the analysis on the cases with $p_{11}p_{22}>0$ or $p_{11}p_{22}<0$. Particularly, the case where $p_{11}p_{22}>0$ is considered as the simple case due to the planar system determined through Eqs. (22) and (23) do not show periodic solutions. These cycles would correspond to the bifurcations of quasiperiodic solutions, noted above as E_3, which originate the so-called 3D torus. Hence, in the $\eta_1-\eta_2$ parameter plane the Hopf bifurcation curve can be plotted (which has a self-intersection at the singularity) as well as two branches of Neimark–Sacker or torus bifurcation curves, T_1 and T_2, where the above-mentioned 2D tori arise [5]. Otherwise, when the complex case is treated, say $p_{11}p_{22}<0$, the normal form of Eqs. (22)–(25) results inadequate to get a complete dynamic study close to non-resonant DH point. However, considering $p_{11}>0$, $p_{22}<0$, defining the variables $\rho=p_{12}/p_{22}$, $\delta=p_{21}/p_{11}$ (it is known that $\rho\delta-1\neq 0$), six regions whose dynamics are qualitatively different [2], can be distinguished in the $\rho-\delta$ plane with $\rho\geqslant\delta$ as can be observed in Fig. 1. Particularly, the solutions coming from the Hopf bifurcations of quasiperiodic solutions, called 3D tori, can only appear in regions I, II and VI. An schematic representation of the bifurcation curves in the neighborhood of the DH singularity associated to region VI is shown in Fig. 2. The axes τ_1,τ_2 are the tangent lines of Hopf bifurcation curves at $\eta=(\eta_1,\ \eta_2)=(0,0)$, which result from Eqs. (22)–(25), namely $\tau_1=\alpha_{11}\eta_1+\alpha_{12}\eta_2=0$, $\tau_2=\alpha_{21}\eta_1+\alpha_{22}\eta_2=0$. Two new curves C and Y, which have not been introduced up to now, are included in this description. The curve C is the bifurcation curve of the equilibriums of type E_3,

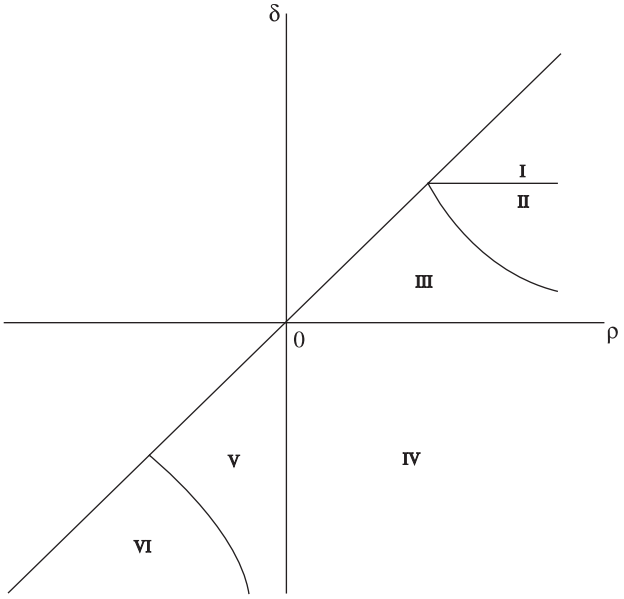

Fig. 1. Characteristic dynamic regions of the $\rho-\delta$ plane, with $\rho \geqslant \delta$, for the non-resonant double Hopf singularity in the complex case.

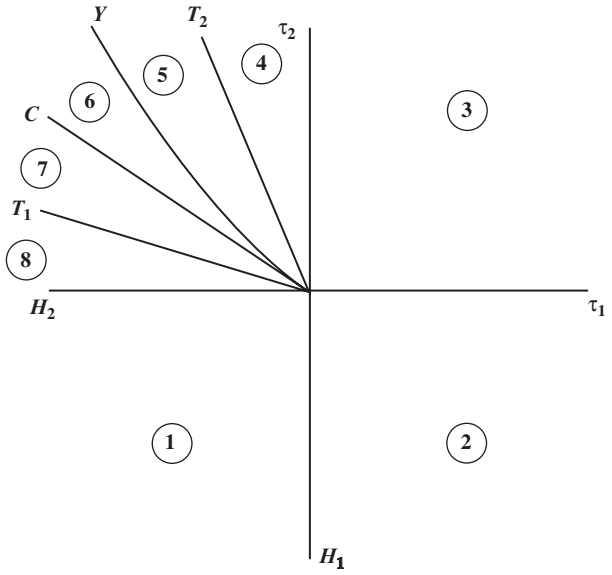

Fig. 2. Schematic representation of the bifurcation curves close to the double Hopf singularity in the case of region VI of Fig. 1 (H_i, $i=1,2$ represent the tangent lines to the Hopf bifurcation branches at criticality while T_i, $i=1,2$ are those to the Neimark–Sacker continuations). The dynamics of the numbered regions are in correspondence with the phase portraits of Fig. 3.

which can be expressed as

$$C=\left\{(\tau_1,\tau_2):\tau_2=-\frac{\delta-1}{\rho-1}\tau_1+O(\tau_1^2),\ \tau_1-\rho\tau_2>0,\ \delta\tau_1-\tau_2>0\right\}, \tag{26}$$

where it is considered $\rho\neq 1$ and $\delta\neq 1$, to avoid the tangency with the lines $H_1:\tau_1=0$ and $H_2:\tau_2=0$. Moreover, Y is the curve where the new periodic solutions disappear, in a heteroclinic bifurcation, whose description requires terms of order higher than those included in the third-order normal form being

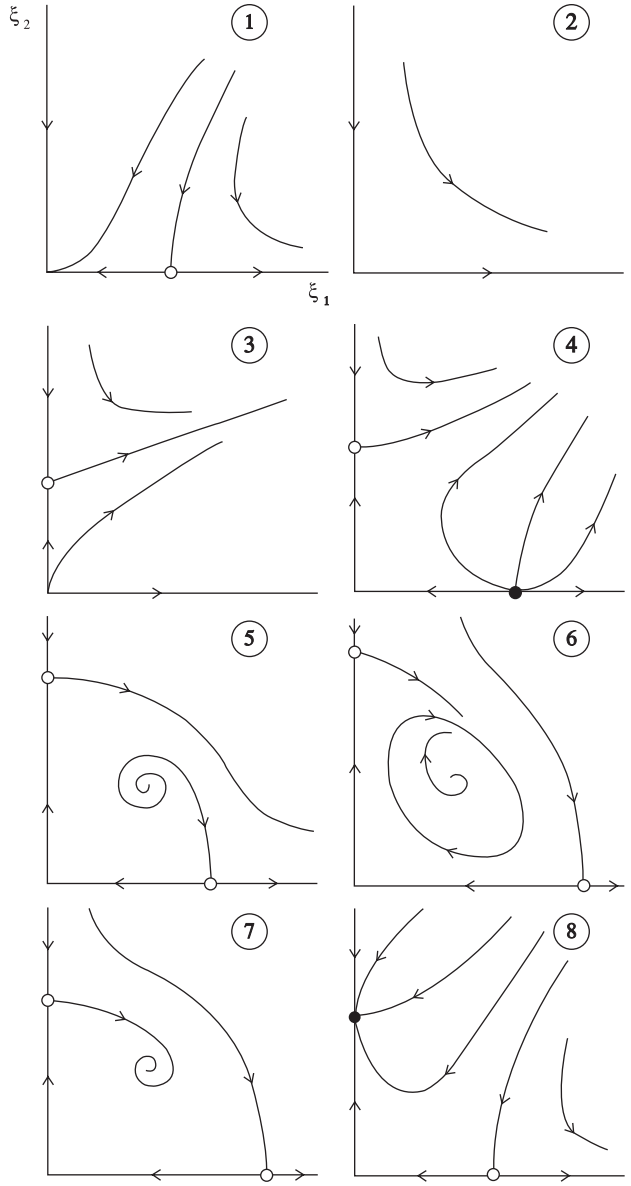

Fig. 3. Phase portraits in the proximity of the non-resonant double Hopf bifurcation point in the complex case corresponding to region VI. The origin is E_0. The singular points on the axes are E_1 or E_2. The singular point outside the coordinate axes is E_3 (see also Fig. 2).

considered. Taking into account the zones indicated in Fig. 2, then their representative phase portraits are shown in Fig. 3, where $\xi_1 = p_{11}r_1^2$, $\xi_2 = -p_{22}r_2^2$. Specifically, a methodology has been given in Ref. [4] starting from the truncated normal form of Eqs. (22)–(25), to determine the tangent lines to the Neimark–Sacker bifurcation curves, T_1 and T_2, whose origin is the non-resonant DH point, as well as to the curve C, where the 3D torus solution emerges.

4. Coupled oscillators with quadratic and cubic nonlinearities

The considered nonlinear system is designed with two coupled resonant circuits as shown in Fig. 4(a), where C_1, C_2 are capacitors, L_1, L_2 are inductances and R is a resistor. Choosing the voltages across the capacitors

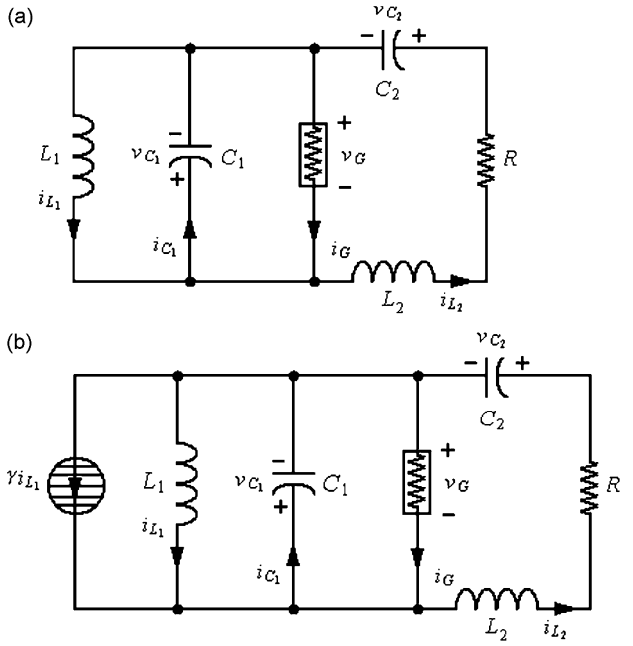

Fig. 4. A doubly coupled electrical circuit: (a) Simple form. (b) With a current-by-current controlled source ($\gamma = \eta_3\eta_1^{-1}$).

and the currents in the inductances as state variables, one obtains

$$\dot{x}_1 = \eta_1(\tfrac{1}{2}x_1 - \alpha_2 x_1^2 - \alpha_3 x_1^3) + \eta_1 x_2 - \eta_1 x_4, \tag{27}$$

$$\dot{x}_2 = -\tfrac{1}{2}\sqrt{2}\,x_1, \tag{28}$$

$$\dot{x}_3 = (\sqrt{2}+1)x_4, \tag{29}$$

$$\dot{x}_4 = (2-\sqrt{2})(x_1 - x_3 - \eta_2 x_4), \tag{30}$$

where $x = (x_1, x_2, x_3, x_4) = (v_{C_1}, i_{L_1}, v_{C_2}, i_{L_2})$, $\eta_1 = 1/C_1$ and $\eta_2 = R$ are independent bifurcation parameters. The constants C_2, L_1 and L_2 have the following values: $C_2 = 1/(\sqrt{2}+1)$, $L_1 = \frac{2}{\sqrt{2}}$ and $L_2 = \frac{1}{2-\sqrt{2}}$. In this case, the conductance is a nonlinear element which can be described according to the current–voltage nonlinear function $i_G = -\frac{1}{2}v_G - \alpha_2 v_G^2 + \alpha_3 v_G^3$, where two additional parameters, α_2 and α_3, are now included.

If a control function which depends on the second variable and a new auxiliary parameter, $u = \eta_3 x_2$, is added to Eq. (27) then the circuit can be synthesized as shown in Fig. 4(b) and now the model is expressed as

$$\dot{x}_1 = \eta_1(\tfrac{1}{2}x_1 - \alpha_2 x_1^2 - \alpha_3 x_1^3) + \chi x_2 - \eta_1 x_4, \tag{31}$$

$$\dot{x}_2 = -\tfrac{1}{2}\sqrt{2}\,x_1, \tag{32}$$

$$\dot{x}_3 = (\sqrt{2}+1)x_4, \tag{33}$$

$$\dot{x}_4 = (2-\sqrt{2})(x_1 - x_3 - \eta_2 x_4), \tag{34}$$

where $\chi = \eta_1 + \eta_3$. It is easy to see that the unique equilibrium point of Eqs. (31)–(34) is $\tilde{x} = 0$, when $\chi = \eta_1 + \eta_3 \neq 0$. It would be noticed that this model has been analyzed previously for the particular case with $(\alpha_2, \alpha_3) = (0, 1)$ in Ref. [5] or even in a simple form, without the current-by-current controlled source in Ref. [4] with $(\alpha_2, \alpha_3) = (0, 1)$ and $\eta_3 = 0$. Since the objective is to analyze its local dynamics as the parameters $\eta = (\eta_1, \eta_2, \eta_3)$ vary, it will be meaningful to know the characteristic polynomial of the linearization of

Eqs. (31)–(34) evaluated at the equilibrium. Such matrix results

$$D_1 = \begin{bmatrix} \frac{1}{2}\eta_1 & \chi & 0 & -\eta_1 \\ -\frac{1}{2}\sqrt{2} & 0 & 0 & 0 \\ 0 & 0 & 0 & \sqrt{2}+1 \\ 2-\sqrt{2} & 0 & -(2-\sqrt{2}) & -(2-\sqrt{2})\eta_2 \end{bmatrix}, \tag{35}$$

and the characteristic polynomial P is

$$P(r) = r^4 + q_3 r^3 + q_2 r^2 + q_1 r + q_0, \tag{36}$$

where

$$q_3 = \eta_2(2-\sqrt{2}) - \frac{\eta_1}{2}, \tag{37}$$

$$q_2 = \frac{\sqrt{2}}{2}(\eta_3 - \eta_1) - (2-\sqrt{2})\frac{1}{2}\eta_1\eta_2 + \sqrt{2} + 2\eta_1, \tag{38}$$

$$q_1 = \chi\eta_2(\sqrt{2}-1) - \frac{\eta_1}{2}\sqrt{2}, \tag{39}$$

$$q_0 = \chi. \tag{40}$$

If the necessary conditions to detect a 1:1 resonant DH point are stated, namely,

$$q_3 = 0, \quad q_2 = 2\omega^2, \quad q_1 = 0, \quad q_0 = \omega^4, \tag{41}$$

for a certain frequency value $\omega > 0$, then it follows that the unique solution exists for

$$\omega^{**} = \sqrt[4]{2}, \quad \eta^{**} = (\eta_1^{**}, \eta_2^{**}, \eta_3^{**}) = (4(2-\sqrt{2}), 2, 2(2\sqrt{2}-3)). \tag{42}$$

Additionally, a Whitney umbrella is described in its neighborhood [5], as can be observed in Fig. 5. This surface, distinctive of this three codimension Hopf degeneracy, collects the Hopf bifurcation points that are close to this singularity. Furthermore, one discovers infinite nearby non-resonant DH points in the space $\eta : \eta_1 - \eta_2 - \eta_3$, which solve the system

$$\omega_1^2 + \omega_2^2 = -\frac{\eta_3^2}{4} + (\sqrt{2}-1)\eta_3 + 3 > 0, \tag{43}$$

$$\omega_1^2\omega_2^2 = \chi = 2, \tag{44}$$

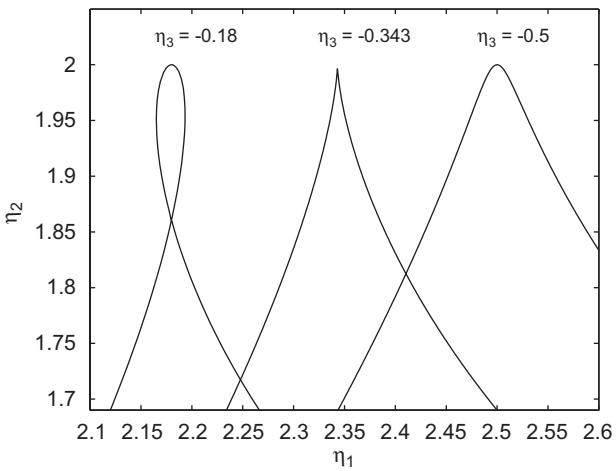

Fig. 5. Characteristic Whitney umbrella sections by varying η_3 close to the 1:1 resonant double Hopf singularity for the model of Eqs. (31)–(34).

where $\pm i\omega_1$, $\pm i\omega_2$ are the eigenvalues of the linearization at the equilibrium, $\eta_2 = \frac{1}{4}\eta_1(2+\sqrt{2})$ and $\eta_1 > 0$. Then, it results $2(2\sqrt{2}-3) < \eta_3 < 2$ (which means that $2\sqrt{2} < \omega_1^2 + \omega_2^2 \leqslant 2(3-\sqrt{2})$). Particularly, the focus will be the analysis of the dynamics close to a non-resonant DH singularity in the case recognized as complex [2], like the one described in Section 4.

4.1. Methodological approach

Following the structure of Eqs. (2) and (3), the system given by Eqs. (31)–(34) can be expressed as a feedback system as follows:

$$A = \begin{bmatrix} 0 & \chi & 0 & -\eta_1 \\ -\frac{1}{2}\sqrt{2} & 0 & 0 & 0 \\ 0 & 0 & 0 & \sqrt{2}+1 \\ 2-\sqrt{2} & 0 & -(2-\sqrt{2}) & -(2-\sqrt{2})\eta_2 \end{bmatrix}, \quad B = \begin{bmatrix} 1 \\ 0 \\ 0 \\ 0 \end{bmatrix}, \tag{45}$$

$$C = B^{\mathrm{T}}, \quad D = [0], \tag{46}$$

and $u = g(e;\eta_1,(\alpha_2,\alpha_3)) = \eta_1(-\frac{1}{2}e - \alpha_2 e^2 + \alpha_3 e^3)$, with $e = -y$.

Thus, one computes the transfer matrix $G = C[s * I - (A + BCD)]^{-1}B$ which results

$$\begin{aligned} G(s;\eta) &= G(s;(\eta_1,\eta_2,\eta_3)) \\ &= \frac{2s(s^2 + (2-\sqrt{2})\eta_2 s + \sqrt{2})}{2s^4 + 2(2-\sqrt{2})\eta_2 s^3 + (\kappa + \sqrt{2}n_3)s^2 + 2(\sqrt{2}-1)\chi\eta_2 s + 2\chi}, \end{aligned} \tag{47}$$

where $\kappa = \kappa(\eta_1) = (4-\sqrt{2})\eta_1 + 2\sqrt{2}$. The equilibrium in the frequency realization yields

$$e = -G(0;(\eta_1,\eta_2,\eta_3))g(e;\eta_1,(\alpha_2,\alpha_3)), \tag{48}$$

whose solution is $\tilde{e} = 0$, if $\chi \neq 0$. Hence, follows that $J = D_1 g|_{\tilde{e}=0} = -\frac{1}{2}\eta_1$. Moreover, the characteristic and unique eigenvalue $\hat{\lambda}$ of GJ evaluated at $s = i\omega$ can be expressed as

$$\hat{\lambda} = (A_1 + iA_2)(A_3 + iA_4)^{-1}, \tag{49}$$

where

$$A_1 = -\eta_1\eta_2\omega^2(2-\sqrt{2}), \quad A_2 = \eta_1\omega(\sqrt{2}-\omega^2), \tag{50}$$

$$A_3 = -2\omega^4 + (\kappa + \sqrt{2}\eta_3)\omega^2 - 2\chi, \tag{51}$$

$$A_4 = 2(2-\sqrt{2})\eta_2\omega^3 - 2(\sqrt{2}-1)\chi\eta_2\omega. \tag{52}$$

If $\eta_3 = -0.18$ (which satisfies $2(2\sqrt{2}-3) < \eta_3 < 2$) and Eqs. (43) and (44) are considered, one obtains the remaining coordinates of the non-resonant DH singularity of this η_3-section and the involved frequencies which result

$$\mathrm{DH}: \eta_1 = 2.18, \quad \eta_2 = 1.860746393, \quad \omega_1 = 1.049424039, \quad \omega_2 = 1.347609270.$$

With this starting point and solving the nonlinear system

$$F_1(\omega,\eta) = \mathrm{Re}(\hat{\lambda}) + 1 = 0, \quad F_2(\omega,\eta) = \mathrm{Im}(\hat{\lambda}) = 0, \tag{53}$$

where the expression of $\hat{\lambda}$ is given by Eq. (49), a continuation of Hopf bifurcation points can be done in the $\eta_1 - \eta_2$ parameter plane. The resultant curve, which appears on the left in Fig. 5, has been also verified with LOCBIF [28]. For completeness, the continuations of Hopf points in the cases $\eta_3 = -0.343$ and -0.5 have been performed. These results are in agreement with the different classical sections of the Whitney umbrella [29] close to the 1:1 resonant DH point found before in Eq. (42).

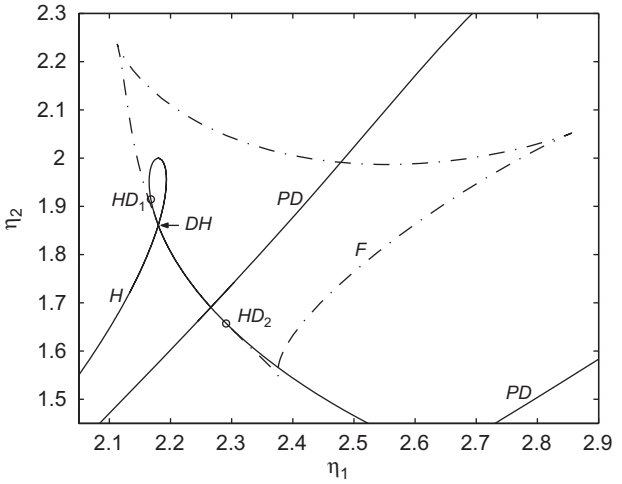

Fig. 6. Hopf bifurcation curve (H), cyclic fold curve (F) (.-) and period-doubling bifurcation curve (PD), in the neighborhood of the non-resonant double Hopf point (DH) with $(\alpha_2, \alpha_3) = (0.6, 1)$, $\eta_3 = -0.18$. ((○) depicts the points HD_i, $i = 1, 2$, which are Hopf degeneracies of type H_{10}).

So far the parameters α_2 and α_3 have been irrelevant. Hence, keeping $\eta_3 = -0.18$ and fixing the values of α_2 and α_3 as $(\alpha_2, \alpha_3) = (0.6, 1)$, one has already computed the Hopf curve in the $\eta_1 - \eta_2$ plane and now the fold bifurcation curve, which looks like a curved triangle, incomplete in one of its sides, and a "line" of period-doubling bifurcations, both obtained entirely with LOCBIF [28], are added. All these curves can be observed in Fig. 6. Particularly, the two points where the cyclic fold curve emerges are Hopf degeneracies such that the curvature coefficient σ_1 vanishes (see Eq. (10) in the hypothesis H3 of Theorem 1), usually noted as H_{10}. These degeneracies give place to the appearance of a pair of limit cycles after performing appropriately small perturbations [1]. Specifically, in the section $\eta_3 = -0.18$, two H_{10} singularities are found and their coordinates are

$$\mathrm{HD}_1 : \eta_1 = 2.167904, \quad \eta_2 = 1.914652, \quad \omega_{\mathrm{HD}_1} = 1.076688, \quad \sigma_{1_{\mathrm{HD}_1}} = -0.135751 * 10^{-6},$$

$$\mathrm{HD}_2 : \eta_1 = 2.291134, \quad \eta_2 = 1.657265, \quad \omega_{\mathrm{HD}_2} = 0.988779, \quad \sigma_{1_{\mathrm{HD}_2}} = -0.128346 * 10^{-7},$$

as indicated in Fig. 6. A similar phenomenon has been observed previously [5] but in that case from the H_{10} degenerate points start two cyclic fold bifurcations which encounter each other in a cusp of limit cycles. Moreover, the special detail of one of these curves close to HD_1 as well as the corresponding non-resonant DH bifurcation (noted as DH in Fig. 6) is shown in Fig. 7 where a new cusp of cyclic fold bifurcations appears. The latter curve has been obtained also with the software LOCBIF.

With the aim of obtaining precise quasianalytical approximations for the limit cycles, the implementation of the graphical Hopf method has been done. Specifically, the modified scheme for the harmonic balances up to the eighth order introduced in Ref. [9] has been used. This methodological choice is based on two basic facts that have been observed: first, sometimes the original iterative formulation does not give results in certain regions of the parameter space where relatively simple dynamics is observed; second, when the results can be obtained with both formulations, those coming from the modified scheme are more precise. The exactness of the different approximations can be measured through the trivial Floquet multipliers and their closeness to the unity, as has been indicated in Ref. [30]. If the case $(\alpha_2, \alpha_3) = (0.6, 1)$, $\eta_3 = -0.18$ is taken up again and the point $(\eta_1, \eta_2) = (2.175, 2)$ is considered (in Fig. 6 the highest point of the Hopf curve is $(2.18, 2)$), the more accurate approximation

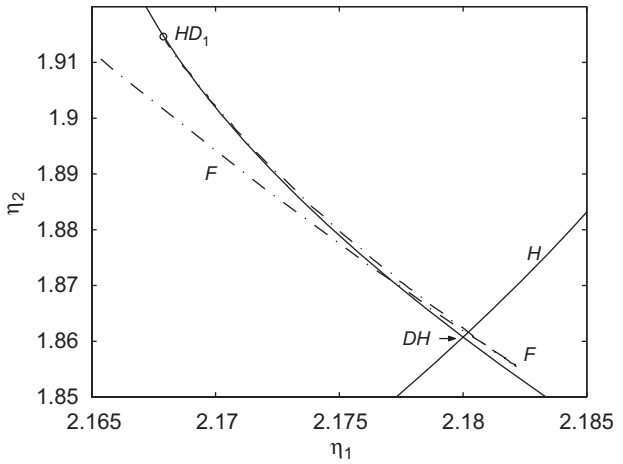

Fig. 7. Blow up of the Hopf bifurcation curve (H) and cyclic fold curve (F) (.-) close to Hopf degeneracy (HD_1) and the non-resonant double Hopf point (DH), with $(\alpha_2, \alpha_3) = (0.6, 1)$, $\eta_3 = -0.18$.

Table 1
Comparison between Floquet or characteristic multipliers of the eighth-order harmonic balance cycle approximation and those from the LOCBIF numerical solution for $(\eta_1, \eta_2) = (2.175, 2)$, with $(\alpha_2, \alpha_3) = (0.6, 1)$, $\eta_3 = -0.18$..

	LOCBIF	HB8
μ_0	1.000017	1.000103642
μ_1	0.9596839	0.9594870295
μ_{2-3}	$0.807212\exp(\pm 0.284314\mathrm{i})$	$0.807178\exp(\pm 0.286248\mathrm{i})$

(up to eight harmonics) results

$$\begin{aligned} x_1 = x_1(t) = & -0.3056785630 * 10^{-1} * \cos(\omega t) \\ & + 0.2220675242 * 10^{-3} * \cos(2\omega t) - 0.3657189113 * 10^{-3} * \sin(2\omega t) \\ & + 0.2007411754 * 10^{-5} * \cos(3\omega t) + 0.9616352086 * 10^{-5} * \sin(3\omega t) \\ & - 0.2298621279 * 10^{-6} * \cos(4\omega t) - 0.1064668729 * 10^{-6} * \sin(4\omega t) \\ & + 0.5930595924 * 10^{-8} * \cos(5\omega t) - 0.2895118666 * 10^{-8} * \sin(5\omega t) \\ & - 0.4070186028 * 10^{-10} * \cos(6\omega t) + 0.1750439323 * 10^{-9} * \sin(6\omega t) \\ & - 0.3009453243 * 10^{-11} * \cos(7\omega t) - 0.3915523582 * 10^{-11} * \sin(7\omega t) \\ & + 0.1379747335 * 10^{-12} * \cos(8\omega t) + 0.3871035960 * 10^{-14} * \sin(8\omega t), \end{aligned} \tag{54}$$

where the approximating frequency is $\omega = 1.165499397$. With this last formula the expression of x_2 can be found from Eq. (32), then x_4 using Eq. (31) and finally x_3 will result from Eq. (33) or (34). Furthermore, a comparison between the associated multipliers and those coming from LOCBIF approximation are shown in Table 1, where there is a remarkable coincidence of results.

On the other hand, if it is considered the point $(\eta_1, \eta_2) = (2.16, 2)$ (a bit more distant from the Hopf curve than the one chosen before), always using the modified scheme for the attainment of the quasianalytical approximations, the trivial Floquet multiplier for the different harmonic balance approximations results $\mu_{0(\mathrm{HB2})} = 0.95790939$, $\mu_{0(\mathrm{HB4})} = 0.97813453$, $\mu_{0(\mathrm{HB6})} = 0.97793528$, $\mu_{0(\mathrm{HB8})} = 1.03997956$, where HB$i$, $i = 1, \ldots, 4$ means the order of the harmonic balance approximation used. It is noticed that there exists a degradation in the results regarding the previous case and this can be explained by the local properties of the graphical Hopf method. Moreover, it must be observed that by increasing the number of harmonics in this

local method does not guarantee a more precise approximation, as can be deduced from the last case where the most accurate approximation comes from the sixth-order harmonic balance.

From now on, the Neimark–Sacker bifurcations which exist in the closeness of the non-resonant DH point will be analyzed and finally, the dynamic interactions between the DH bifurcation and the Gavrilov–Guckenheimer singularity will be considered.

4.2. Neimark–Sacker bifurcations of cycles

The detection of the Neimark–Sacker bifurcation using the graphical Hopf theorem is pursued in this subsection. Returning to the case $(\alpha_2, \alpha_3) = (0.6, 1)$, $\eta_3 = -0.18$ and fixing the parameter $\eta_2 = 1.855$ (taking into account that the non-resonant DH point of the considered section has coordinates $(\eta_1, \eta_2) = (2.18, 1.860746393)$) then the parameter η_1 is varied continuously in the neighborhood of the studied singularity (see Fig. 6). Thereby, it is stated that two values of η_1 exist, namely, $\eta_{1(1)} = 2.178581096$ and $\eta_{1(2)} = 2.181757160$ where two branches of periodic solutions appear, with frequencies $\omega_{1(1)} = 1.350772072$ and $\omega_{1(2)} = 1.046966832$, respectively.

If the evolution of the multipliers of a generic cycle, which arises at $\eta_{1(1)}$ is examined through its most precise approximation (in this case, the one obtained using eighth order (HB8)), a Neimark–Sacker bifurcation of cycles is detected when $\eta_1 = 2.18316$, as can be observed in Table 2. On the other hand, LOCBIF finds this singularity at $\eta_{1(\mathrm{LOCBIF})} = 2.183149$.

Analogously, if a continuation of the limit cycles which start at $\eta_{1(2)}$ is performed considering HB8 approximations, a second Neimark–Sacker bifurcation of cycles is found at $\eta_1 = 2.18187$, whereas LOCBIF detects this singularity for $\eta_{1(\mathrm{LOCBIF})} = 2.181878$. By means of Table 3 it can be checked the last determination through the behavior of the characteristic or Floquet multipliers.

The detection of both Neimark–Sacker bifurcations of cycles that has been carried out confirms once again the existence of two branches of that type of cyclic bifurcations, next to the non-resonant DH singularity.

4.3. Neimark–Sacker branch continuation

Because of the quality of the results obtained in the previous subsection in relation with the detection of Neimark–Sacker bifurcation of cycles and repeating the executed procedure for a certain rank of values η_2, $\eta_2 < 1.86074$, a continuation of Neimark–Sacker bifurcations has been built around the DH bifurcation point $(\eta_1, \eta_2) = (2.18, 1.860746393)$ as it is shown in Fig. 8, where the cyclic fold curve has been neglected just to give more clarity to the presentation (see, for comparison, Figs. 7 and 8). The Neimark–Sacker right branch (*NS* in Fig. 8) can be found through quasianalytical expressions and the evolution of the Floquet multipliers. This

Table 2
Detection of a Neimark–Sacker bifurcation of cycles for $\eta_2 = 1.855$, with $(\alpha_2, \alpha_3) = (0.6, 1)$, $\eta_3 = -0.18$..

	$\eta_1 = 2.18316$	$\eta_1 = 2.18317$
μ_0	1.000157091	1.000157735
μ_{1-2}	$1.000013\exp(\pm 1.485728\mathrm{i})$	$0.999999\exp(\pm 1.485875\mathrm{i})$
μ_3	0.9732324960	0.9731774115

Table 3
Detection of a second Neimark–Sacker bifurcation of cycles for $\eta_2 = 1.855$, with $(\alpha_2, \alpha_3) = (0.6, 1)$, $\eta_3 = -0.18$..

	$\eta_1 = 2.18187$	$\eta_1 = 2.18188$
μ_0	1.001122162	1.001260163
μ_{1-2}	$1.000540\exp(\pm 1.871959\mathrm{i})$	$0.999385\exp(\pm 1.876214\mathrm{i})$
μ_3	0.9993793493	0.9992795556

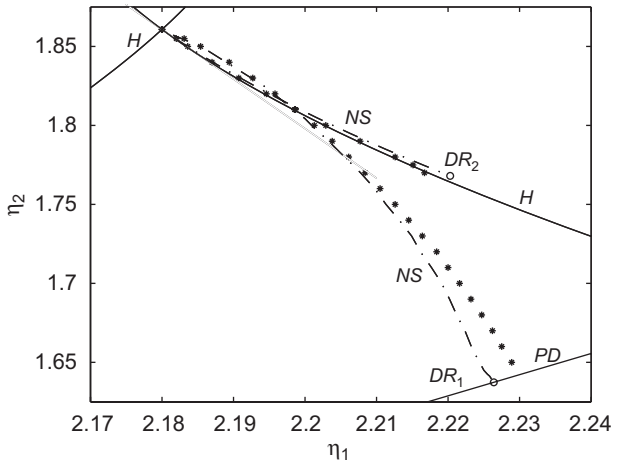

Fig. 8. Neimark–Sacker bifurcation curves (*NS*) close to non-resonant double Hopf point for $(\alpha_2, \alpha_3) = (0.6, 1)$, $\eta_3 = -0.18$. (LOCBIF (.-), graphical Hopf method (*), period-doubling bifurcation curve (*PD*), Hopf bifurcation curve (*H*), the points DR_i, $i = 1, 2$ are indicated with (○)).

branch (up to eighth-order approximation) finishes at a singularity with a double Floquet multiplier -1, known as resonance 1:2 [2]. This has been noted as $\mathrm{DR}_1 : (\eta_1, \eta_2) = (2.2264, 1.6373)$, which belongs also to a period-doubling bifurcation curve. This Neimark–Sacker branch results from the cyclic bifurcation of the left branch of the Hopf curve (associated to the larger critical frequency $\omega_2 = 1.347609270$). These outcomes have been checked also by using LOCBIF. As can be easily seen in Fig. 8 there is a discrepancy between LOCBIF determination of the lower part of the *NS* curve approaching DR_1 singularity and its determination using the frequency domain method. The inclusion of more harmonics such as in Ref. [31], who have used up to 21 harmonics, may help to locate more accurately the mentioned singularity.

For the location of the second branch of Neimark–Sacker curve and due to the required detail, it has been necessary to use normal forms [2,27] at first. Therefore, the results in Ref. [15] and more recently in Ref. [4] have allowed to compute the slopes of the so-called critical lines, particularly that of the tangent line to the approximation of the left *NS* branch, which can be obtained through normal forms. This procedure has been attained by means of the adaptation of the algorithms published in Ref. [4]. Recalling that $\eta_3 = -0.18$, the non-resonant DH singularity (noted as *DH* in the figures) is located at $\eta = (\eta_1, \eta_2) = (2.18, 1.860746393)$ and the involved frequencies are $\omega_1 = 1.049424039$ and $\omega_2 = 1.347609270$. With the established goal, first η_1 is replaced by $(\eta_1 + 2.18)$ and η_2 by $(\eta_2 + 1.860746393)$ in Eqs. (31)–(34) to set up the dynamic analysis of the DH bifurcation at the origin of the $\eta_1 - \eta_2$ plane. Then, it is necessary to fulfill a change of coordinates in order to apply the correspondent algorithm.

Calling $z = [z_1 \;\; z_2 \;\; z_3 \;\; z_4]^{\mathrm{T}}$ and considering the following linear change of variables $x = Mz$ where

$$M = \begin{bmatrix} 1 & 0 & 1 & 0 \\ 0 & \dfrac{\sqrt{2}}{2\omega_1} & 0 & \dfrac{\sqrt{2}}{2\omega_2} \\ \dfrac{K}{\omega_1 \bar{\eta}_1} W_1 & -\dfrac{K}{2\omega_1} & \dfrac{K}{\omega_2 \bar{\eta}_1} W_2 & -\dfrac{K}{2\omega_2} \\ \dfrac{1}{2} & \dfrac{1}{\bar{\eta}_1} W_1 & \dfrac{1}{2} & \dfrac{1}{\bar{\eta}_1} W_2 \end{bmatrix} \tag{55}$$

with $K = \sqrt{2} + 1$, $\bar{\eta}_1 = 2.18$ and $W_i = \sqrt{2}/\omega_i - \omega_i$, $i = 1, 2$, Eqs. (31)–(34) become

$$\dot{z} = \bar{F}(z; \eta) = \bar{A}z + \bar{G} + \bar{H}, \tag{56}$$

where

$$\dot{z}=\begin{bmatrix}\dot{z}_1\\ \dot{z}_2\\ \dot{z}_3\\ \dot{z}_4\end{bmatrix},\quad \bar{F}=\begin{bmatrix}\bar{F}_1(z;\eta)\\ \bar{F}_2(z;\eta)\\ \bar{F}_3(z;\eta)\\ \bar{F}_4(z;\eta)\end{bmatrix},\quad \bar{A}=\begin{bmatrix}0 & \omega_1 & 0 & 0\\ -\omega_1 & 0 & 0 & 0\\ 0 & 0 & 0 & \omega_2\\ 0 & 0 & -\omega_2 & 0\end{bmatrix}, \tag{57}$$

$$\bar{G}=\begin{bmatrix}\bar{G}_1(z;\eta)\\ \bar{G}_2(z;\eta)\\ \bar{G}_3(z;\eta)\\ \bar{G}_4(z;\eta)\end{bmatrix}\quad\text{and}\quad \bar{H}=\begin{bmatrix}\bar{H}_1(z;\eta)\\ \bar{H}_2(z;\eta)\\ \bar{H}_3(z;\eta)\\ \bar{H}_4(z;\eta)\end{bmatrix}. \tag{58}$$

The expressions of the functions $\bar{G}_i$, $i=1,\ldots,4$ result

$$\bar{G}_i(z;\eta)=\sum a_{ijk}\eta_j z_k,\quad k=1,\ldots,4;\ \ j=1,2 \tag{59}$$

for certain numerical coefficients a_{ijk}, namely

$$\bar{G}_1(z;\eta)=0.235109\eta_1 z_2+0.289602\eta_1 z_4, \tag{60}$$

$$\begin{aligned}\bar{G}_2(z;\eta)=&-0.859428\eta_1 z_2-1.058627\eta_1 z_4-3.200717\eta_2 z_1-0.875602\eta_2 z_2\\&-3.200717\eta_2 z_3+0.875602\eta_2 z_4+1.600358\sqrt{2}\eta_2 z_1\\&+0.437801\sqrt{2}\eta_2 z_2+1.600358\sqrt{2}\eta_2 z_3-0.437801\sqrt{2}\eta_2 z_4,\end{aligned} \tag{61}$$

$$\bar{G}_3(z;\eta)=0.301913\eta_1 z_2+0.371891\eta_1 z_4, \tag{62}$$

$$\begin{aligned}\bar{G}_4(z;\eta)=&1.103627\eta_1 z_2+1.359428\eta_1 z_4+4.110174\eta_2 z_1+1.124397\eta_2 z_2\\&+4.110174\eta_2 z_3-1.124397\eta_2 z_4-2.055087\sqrt{2}\eta_2 z_1\\&-0.562198\sqrt{2}\eta_2 z_2-2.055087\sqrt{2}\eta_2 z_3+0.562198\sqrt{2}\eta_2 z_4,\end{aligned} \tag{63}$$

and

$$\bar{H}_1(z;\eta)=\frac{(-\sqrt{2}+\omega_2^2)\omega_1^2 D^*}{\sqrt{2}C^*},\quad \bar{H}_2(z;\eta)=-\frac{\eta_1\omega_1 D^*}{2C^*}, \tag{64}$$

$$\bar{H}_3(z;\eta)=-\frac{(-\sqrt{2}+\omega_1^2)\omega_2^2 D^*}{\sqrt{2}C^*},\quad \bar{H}_4(z;\eta)=\frac{\eta_1\omega_2 D^*}{2C^*}, \tag{65}$$

where $C^*=\omega_2^2-\omega_1^2$ and $D^*=(\eta_1+2.18)(0.6(z_1+z_3)^2+(z_1+z_3)^3)$.

So, considering $(\eta_1,\eta_2)=(0,0)$, one obtains a planar system similar to the one that comes from Eqs. (22)–(25) where these equations are related with the frequencies ω_1 and ω_2, $\omega_1<\omega_2$ (notice that the notation of Ref. [2] is used in this case), respectively, and

$$p_{11}=0.03931641402,$$

$$p_{12}=0.2231297896,$$

$$p_{21}=-1.713632828,$$

$$p_{22}=-0.9290648940,$$

and the coefficients of the parameters η_1, η_2, according to the formulas established in Ref. [15], result

$$\alpha_{11}=\frac{1}{2}\left(\frac{\partial^2\bar{F}_1}{\partial z_1\partial\eta_1}+\frac{\partial_2^2\bar{F}_2}{\partial z_2\partial\eta_1}\right)=-0.4297142244, \tag{66}$$

$$\alpha_{12} = \frac{1}{2}\left(\frac{\partial_1^2 \bar{F}_1}{\partial z_1 \partial \eta_2} + \frac{\partial^2 \bar{F}_2}{\partial z_2 \partial \eta_2}\right) = -0.1282290000, \tag{67}$$

$$\alpha_{21} = \frac{1}{2}\left(\frac{\partial^2 \bar{F}_3}{\partial z_3 \partial \eta_1} + \frac{\partial^2 \bar{F}_4}{\partial z_4 \partial \eta_1}\right) = 0.6797142250, \tag{68}$$

$$\alpha_{22} = \frac{1}{2}\left(\frac{\partial^2 \bar{F}_3}{\partial z_3 \partial \eta_2} + \frac{\partial^2 \bar{F}_4}{\partial z_4 \partial \eta_2}\right) = -0.1646642193. \tag{69}$$

Moreover, using the computed values of p_{ij}, α_{ij}, $i,j = 1,2$ and the equations given in Ref. [4], the expressions of the critical lines L_3 and L_4 passing through DH bifurcation can be attained

$$L_3 : \eta_2 = -3.137102640(\eta_1 - 2.18) + 1.860746393, \tag{70}$$

$$L_4 : \eta_2 = -1.588250939(\eta_1 - 2.18) + 1.860746393. \tag{71}$$

The determination of the line L_3 guides the search of the remaining (left) Neimark–Sacker branch, which has been built, finally, with the suggested methodology. The difficulty of its determination is associated with its proximity to the right branch of the Hopf curve (associated to the smaller critical frequency $\omega_1 = 1.049424039$) in the considered η_3-section. The comparison between the frequency domain results and the critical lines can be seen in Fig. 9. Moreover, an islet of period-doubling bifurcations has been also detected (see Fig. 10(b)) much closer and above the right Hopf branch. This islet has been obtained with LOCBIF, and one of its points is noted as DR_2: $(\eta_1, \eta_2) = (2.2203, 1.7680)$. See also Fig. 10(a) to appreciate its proximity to the DH singularity. The DR_2 point indicates the end of the Neimark–Sacker branch whose tangent line is L_3. It is very illustrative to appreciate the scale on the coordinate axes for Figs. 8–10 as well as the limited approximations on normal forms and the frequency domain methods compared to the continuation software LOCBIF.

If one takes into account that $p_{11}p_{22} < 0$, it can be inferred that the analyzed case with $\eta_3 = -0.18$ agrees with the non-resonant double case singularity of complex type described in Section 4. Matching the attained planar system (here $\omega_1 < \omega_2$ in the notation of Ref. [2]), now $\rho = p_{21}/p_{11} < 0$, $\delta = p_{12}/p_{22} < 0$ and $\rho\delta > 1$, the identified dynamics is related with the case VI in Fig. 1, whose detail can be observed in Figs. 2 and 3 and involves the Hopf bifurcation of a 2D torus, which represents the existence of a 3D torus. In this way, using again the outcomes of Ref. [4] for the determination of L_5, the tangent line of the curve C where the

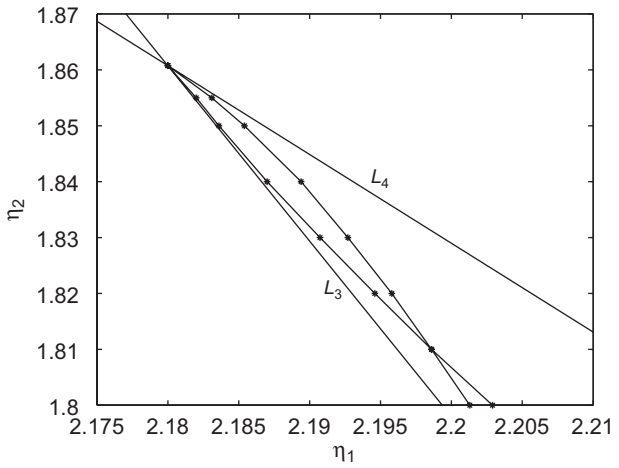

Fig. 9. Comparison between the graphical Hopf method (-*-) and normal forms theory (–) for the Neimark–Sacker curves of the system of Eqs. (31)–(34), with $(\alpha_2, \alpha_3) = (0.6, 1)$, $\eta_3 = -0.18$. (L_3 and L_4, which are obtained through the algorithm in Ref. [4], denote the linear approximations of the Neimark–Sacker curves).

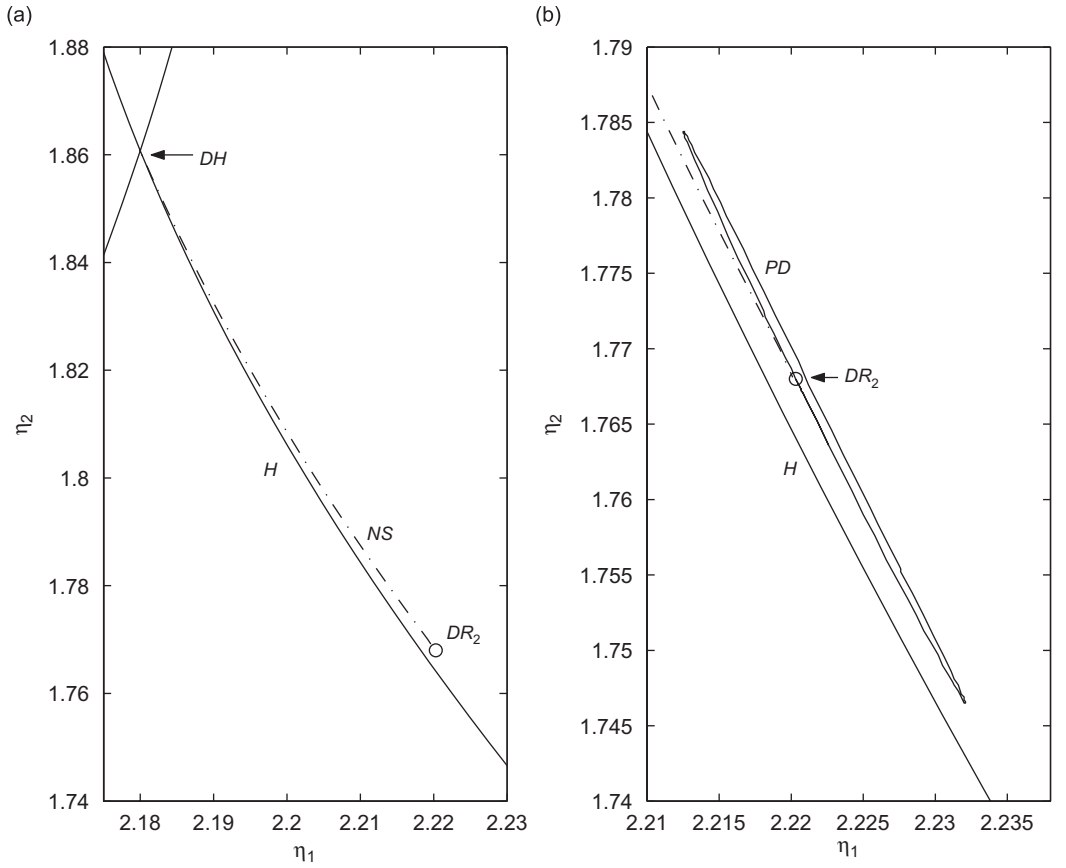

Fig. 10. (a) Left Neimark–Sacker bifurcation curve *NS* (-.) for $(\alpha_2, \alpha_3) = (0.6, 1)$, $\eta_3 = -0.18$. (b) Blow up of (a) in which the Neimark–Sacker curve ends at the point DR_2 (○) which belongs to a period-doubling bifurcation islet (*PD*) (Hopf bifurcation curve (*H*)).

quasiperiodic solutions bifurcate, results:

$$L_5 : \eta_2 = -3.093217706(\eta_1 - 2.18) + 1.8607446393, \tag{72}$$

that is located consistently between the former lines L_4 and L_3, but almost attached to the last one. Then, in the $\eta_1 - \eta_2$ parameter plane, the dynamics close to the selected non-resonant DH singularity is organized according to the bifurcation curves and regions established in Fig. 11.

A similar dynamic situation appears when it is considered $\eta_3 = -0.22$ but the benefit in this case is that the line L_5 is placed a bit more separate from the critical lines L_3 and L_4, which allows to deepen the analysis in relation with the bifurcation curve C of the quasiperiodic solutions. When $\eta_3 = -0.22$ and solving Eqs. (43) and (44), follows that the non-resonant DH singularity $\overline{\mathrm{DH}}$ and its critical frequencies are

$$\overline{\mathrm{DH}} : \eta_1 = 2.22, \quad \eta_2 = 1.894888527, \quad \bar{\omega}_1 = 1.065654287, \quad \bar{\omega}_2 = 1.327084759.$$

Naming $\bar{L}_1$ and $\bar{L}_2$ the tangent lines to the Hopf branches, which cross through $\overline{\mathrm{DH}}$, $\bar{L}_3$ and $\bar{L}_4$ the tangent lines to the Neimark–Sacker branches that arise at the singularity, and at last $\bar{L}_5$ the tangent line to the curve C where the toroidal solutions bifurcate, the dynamic scenario can be understood globally. The slopes $\bar{m}_i$ for these lines, obtained like in the case $\eta_3 = -0.18$ through the algorithm in Ref. [4], are: $\bar{m}_1 = -3.955904$, $\bar{m}_2 = 4.715567$, $\bar{m}_3 = -3.349711$, $\bar{m}_4 = -1.205744$, and $\bar{m}_5 = -3.186850$, being the last three plotted in Fig. 12, together with the estimations of the Neimark–Sacker branches coming through the graphical Hopf method by using eighth-order harmonic balance. The determination of the line $\overline{L}_5$ has allowed to obtain

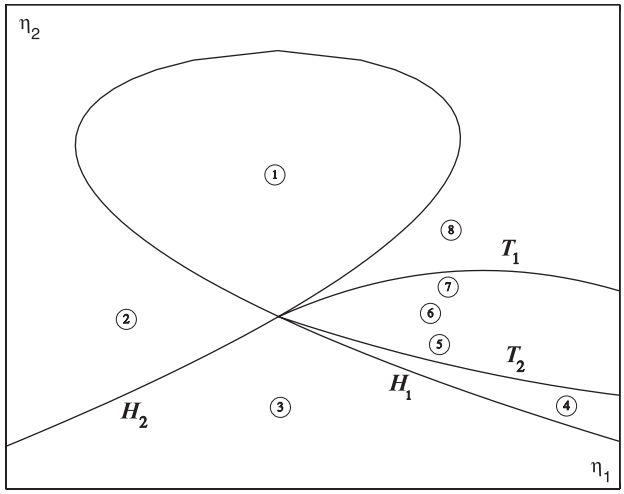

Fig. 11. Qualitative dynamic portrait close to non-resonant double Hopf singularity (complex case) in the parameter plane $\eta_1-\eta_2$ for the system of Eqs. (31)–(34), with $(\alpha_2,\alpha_3)=(0.6,1)$, $\eta_3=-0.18$. (H_i, $i=1,2$, are the Hopf branches; $T_i=NS_i$, $i=1,2$, are the Neimark–Sacker branches and the numbers in the different regions correspond to the phase portraits described in Fig. 3.)

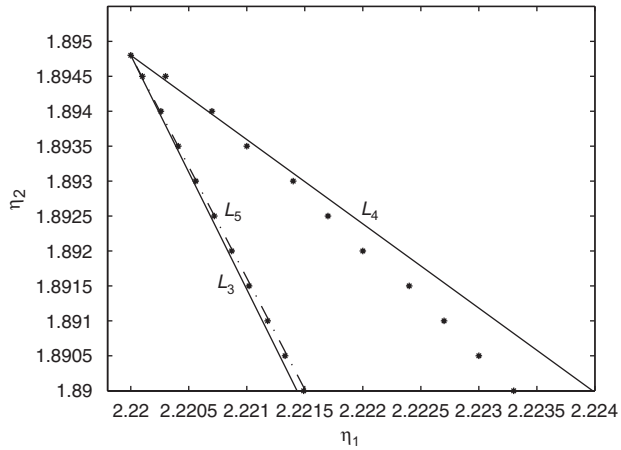

Fig. 12. Comparison between the graphical Hopf method (*) and normal forms theory (–) for the Neimark–Sacker bifurcation curves of Eqs. (31)–(34) which arise at $\overline{\mathrm{DH}}$, together with the line $L_5=\overline{L}_5$ (-.), when $(\alpha_2,\alpha_3)=(0.6,1)$, $\eta_3=-0.22$. ($L_3=\overline{L}_3$ and $L_4=\overline{L}_4$ denote the linear approximations of the Neimark–Sacker curves which are obtained through the algorithm in Ref. [4].)

simulations close to $\overline{\mathrm{DH}}$ confirming the existence of solutions which involve three oscillatory modes. This has been reported recently [32].

4.4. One complex configuration

Returning to the case $\eta_3=-0.18$ and with the aid of the software LOCBIF the continuation of the period-doubling bifurcation curve, where the point DR_1 appears, gives a new closed curve (see Fig. 13), which has an additional singularity $\mathrm{DR}_3:(\eta_1,\eta_2)=(2.001972,0.9130627)$, with the same characteristics as DR_1. Inside this big island, other Neimark–Sacker curve is encountered as well as other higher-order resonances of limit cycles, which confines a region where chaotic behavior could be detected. In the rest of this subsection it is attempted to investigate the reasons for the appearance of the last detected singularity and what its associated local dynamics is.

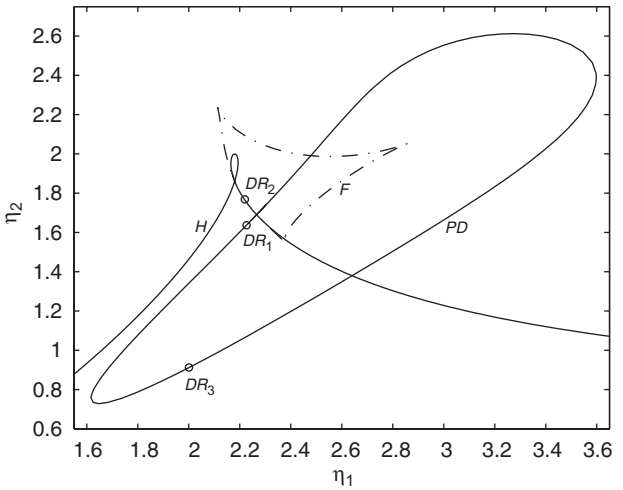

Fig. 13. Continuation of Hopf bifurcation points (H), cyclic fold (F) (.-) and period-doubling or flip (PD) curves in the $\eta_1-\eta_2$ parameter plane for Eqs. (31)–(34) with $(\alpha_2,\alpha_3)=(0.6,1)$ and $\eta_3=-0.18$ (the points $\mathrm{DR}_i,\ i=1,2,3$ are indicated with (○)).

Moreover, considering the expression of the characteristic polynomial of the linearization of Eqs. (31)–(34), which appears in Eqs. (36) and (37)–(40) under the condition $\eta_3=-0.18$, follows that if

$$q_0=\chi=\eta_1+\eta_3=0, \tag{73}$$

then the linearization has at least one zero eigenvalue, implying $\eta_1=0.18$. Analyzing the remaining coefficients results

$$q_3=\eta_2(2-\sqrt{2})-0.09, \tag{74}$$

$$q_2=0.09(2-\sqrt{2})(2\eta_2-1)+\sqrt{2}, \tag{75}$$

$$q_1=-\tfrac{1}{2}0.18\sqrt{2}=-0.09\sqrt{2}. \tag{76}$$

Given that $q_1\neq 0$, it can be affirmed that the zero eigenvalue is always simple. Now, it is wondered if is possible to find a point of the $\eta_1-\eta_2$ plane where the other three eigenvalues are: a pair of imaginary pure $\pm i\omega$ and a real non-zero eigenvalue, noted as b. In these terms, the nonlinear system satisfies

$$q_3=-b,\quad q_2=\omega^2,\quad q_1=-b\omega^2, \tag{77}$$

whose unique allowable solution results: $\eta_2=0.01060767$, $b=0.08378616$ and $\omega=1.23251607$. Thus, another Hopf degeneracy known as fold-Hopf or Gavrilov–Guckenheimer is established at the point $(\eta_1,\eta_2)=(0.18,0.01060767)$, whose critical frequency is $\omega=1.23251607$. It is known that the existence of fold-Hopf singularity is related with the appearance of quasiperiodic solutions, coming from Neimark–Sacker bifurcation curves [2]. In this case, this singularity appears at the intersection of a static bifurcation curve whose equation is $\eta_1=0.18$, the Hopf bifurcation curve and a new Neimark–Sacker cyclic bifurcation curve, which ends at DR_3. Analogous situations have been analyzed in Ref. [33] as well as in Ref. [6], in different applications. The mentioned curves have been approximated using the frequency methodology and, particularly, the Neimark–Sacker bifurcation curve compared with the one built by LOCBIF. All these curves can be observed in Fig. 14. Finally, a global representation of the $\eta_1-\eta_2$ plane where the non-resonant DH and the Gavrilov–Guckenheimer singularities interact together with the referred curves, is shown in Fig. 15.

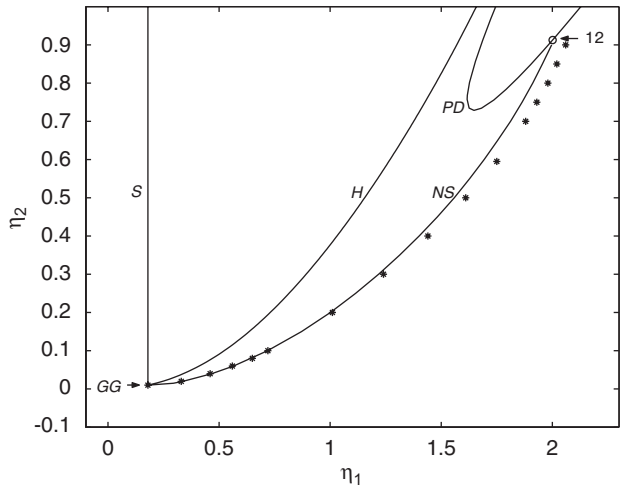

Fig. 14. Bifurcation curves that collapse at Gavrilov–Guckenheimer (*GG*) singularity in Eqs. (31)–(34) when $(\alpha_2, \alpha_3) = (0.6, 1)$, $\eta_3 = -0.18$. (Hopf curve (*H*), period-doubling bifurcation curve (*PD*), static bifurcation curve (*S*), Neimark–Sacker bifurcation curve (*NS*) with LOCBIF (–), with the frequency methodology (*), (○) represents DR_3, which is one 1:2 resonance.)

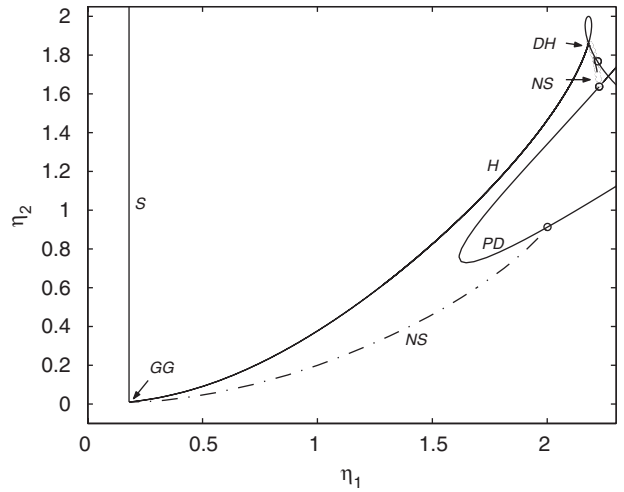

Fig. 15. Interactions between the non-resonant double Hopf (*DH*) and the Gavrilov–Guckenheimer (*GG*) singularities when $(\alpha_2, \alpha_3) = (0.6, 1)$, $\eta_3 = -0.18$. (Hopf curve (*H*), period-doubling bifurcation curve (*PD*), static bifurcation curve (*S*), Neimark–Sacker bifurcation curves (*NS*) (.-), (○) denotes the points DR_i, $i = 1, 2, 3$.)

5. Conclusions

The application of the methodology in the so-called frequency domain and the Floquet theory has permitted us to analyze the neighborhood of the non-resonant DH bifurcation, specially through the computation of Neimark–Sacker bifurcation curves. This result has been also verified with the theory of normal forms and extensive simulations. The detection of other limit cycle bifurcations (fold and period-doubling) has completed the analyzed scenario. The cyclic fold bifurcations are connected to some Hopf degeneracies where the stability index in Eq. (10) vanishes. A closed curve of period-doubling bifurcations as well as the presence of a 3D torus alert about the possibility of the existence of chaotic solutions in the vicinity of these singularities. Moreover, on the period-doubling bifurcation curves some resonance points are detected and these are the birth of singular toroidal motions. A Gavrilov–Guckenheimer singularity has been obtained close to a non-resonant DH bifurcation. The frequency domain methodology is useful in order to compute some of the cyclic

bifurcations in the unfolding of the multiple Hopf singularities, specially those coming from Neimark–Sacker bifurcations which still seem very promissory to end up in chaotic motion after a cascading of some of them via a small parameter change [23]. Finally, this simple circuit model appears to be an interesting and useful vehicle to explore other bifurcating (complex) scenarios.

Acknowledgments

G.R.I. acknowledges Universidad Nacional del Comahue (04/E068). J.L.M. appreciates the support of CONICET (PIP 5032), ANPCyT (PICT-2006-00828) and SGCyT of the Universidad Nacional del Sur (24/K041).

References

[1] M. Golubitsky, W.F. Langford, Classification and unfoldings of degenerate Hopf bifurcations, *Journal of Differential Equations* 41 (1981) 375–415.
[2] Y. A. Kuznetsov, *Elements of Applied Bifurcation Theory*, *Applied Mathematics Sciences*, third ed., vol. 112, Springer, New York, 2004.
[3] P. Yu, Y. Yuan, The simplest normal form for the singularity of a pure imaginary pair and a zero eigenvalue, *Dynamics of Continuous, Discrete and Impulsive Systems, Series B: Applications and Algorithms* 8 (2001) 219–249.
[4] P. Yu, Analysis on double Hopf bifurcation using computer algebra with the aid of multiple scales, *Nonlinear Dynamics* 27 (2002) 19–53.
[5] G.R. Itovich, J.L. Moiola, Double Hopf bifurcation analysis using frequency domain methods, *Nonlinear Dynamics* 39 (2005) 235–258.
[6] F.I. Robbio, D.M. Alonso, J.L. Moiola, Detection of limit cycle bifurcations using harmonic balance methods, *International Journal of Bifurcation and Chaos* 14 (2004) 3647–3654.
[7] E. Freire, E. Gamero, A.J. Rodríguez-Luis, A. Algaba, A note on the triple-zero linear degeneracy: normal forms, dynamical and bifurcation behaviors of an unfolding, *International Journal of Bifurcation and Chaos* 12 (2002) 2799–2820.
[8] A.I. Mees, L.O. Chua, The Hopf bifurcation theorem and its applications to nonlinear oscillations in circuits and systems, *IEEE Transactions on Circuits and Systems* 26 (1979) 235–254.
[9] J.L. Moiola, G. Chen, *Hopf Bifurcation Analysis—A Frequency Domain Approach*, World Scientific Publishing Co., Singapore, 1996.
[10] G.R. Itovich, J.L. Moiola, Characterization of dynamic bifurcations in the frequency domain, *International Journal of Bifurcation and Chaos* 12 (2002) 87–101.
[11] E.H. Abed, J.H. Fu, Local feedback stabilization and bifurcation control, II. Stationary bifurcation, *Systems Control Letters* 8 (1987) 467–473.
[12] E.H. Abed, J.H. Fu, Local feedback stabilization and bifurcation control, I. Hopf bifurcation, *Systems Control Letters* 7 (1986) 11–17.
[13] G. Chen, J.L. Moiola, H.O. Wang, Bifurcation control: theories, methods, and applications, *International Journal of Bifurcation and Chaos* 10 (2000) 511–548.
[14] A. Tesi, E.H. Abed, R. Genesio, H.O. Wang, Harmonic balance analysis of period-doubling bifurcations with implications for control of nonlinear dynamics, *Automatica* 32 (1996) 1255–1271.
[15] K. Huseyin, P. Yu, On bifurcations into nonresonant quasi-periodic motions, *Applied Mathematics Modelling* 12 (1988) 189–201.
[16] J.C. Ji, Nonresonant Hopf bifurcations of a controlled van der Pol–Duffing oscillator, *Journal of Sound and Vibration* 297 (2006) 183–199.
[17] J. Rasmussen, E. Mosekilde, C. Reick, Bifurcations in two coupled Rössler systems, *Mathematics and Computers in Simulation* 40 (1996) 247–270.
[18] V. Gattulli, F. Di Fabio, A. Luongo, One to one resonant double Hopf bifurcation in aeroelastic oscillators with tuned mass dampers, *Journal of Sound and Vibration* 262 (2003) 201–217.
[19] P.A. Chamara, B.D. Coller, A study of double flutter, *Journal of Fluids and Structures* 19 (2004) 863–879.
[20] J. Lopez, F. Marques, Small aspect ratio Taylor–Couette flow: onset of a very-low-frequency three-torus state, *Physical Review E* 68 (2003) 036302, 9pp.
[21] J.M. Tuwankotta, Widely separated frequencies in coupled oscillators with energy-preserving quadratic nonlinearity, *Physica D* 182 (2003) 125–149.
[22] Q. Bi, Dynamical analysis of two coupled parametrically excited van der Pol oscillators, *International Journal of Non-Linear Mechanics* 39 (2004) 33–54.
[23] D.J. Albers, J.C. Sprott, Routes to chaos in high-dimensional dynamical systems: a qualitative numerical study, *Physica D* 223 (2006) 194–207.
[24] G.W. Luo, Y.L. Zhang, Y.D. Chu, J.G. Zhang, Codimension two bifurcations of fixed points in a class of vibratory systems with symmetrical rigid stops, *Nonlinear Analysis: Real World Applications* 8 (2007) 1272–1292.

[25] G.L. Wen, D.L. Xu, Feedback control of Hopf–Hopf interaction bifurcation with development of torus solutions in high dimensional maps, *Physics Letters A* 321 (2004) 24–33.
[26] A.I. Mees, *Dynamics of Feedback Systems*, Wiley, Chichester, UK, 1981.
[27] J. Guckenheimer, P. Holmes, *Nonlinear Oscillations, Dynamical Systems and Bifurcations of Vector Fields*, *Applied Mathematics Sciences*, fourth ed., vol. 42, Springer, New York, 1993.
[28] A.I. Khibnik, Y.A. Kuznetsov, V.V. Levitin, E.V. Nikolaev, Continuation techniques and interactive software for bifurcation analysis of ODE's and iterated maps, *Physica D* 62 (1993) 360–371.
[29] W.J.F. Govaerts, J. Guckenheimer, A.I. Khibnik, Defining functions for multiple Hopf bifurcations, *SIAM Journal of Numerical Analysis* 34 (1997) 1269–1288.
[30] R. Seydel, *Practical Bifurcation and Stability Analysis*, *Interdisciplinary Applied Mathematics*, vol. 5, Springer, New York, 1994.
[31] F. Bonani, M. Gilli, Analysis of stability and bifurcations of limit cycles in Chua's circuit through the harmonic-balance approach, *IEEE Transactions on Circuits and Systems I—Fundamental Theory and Applications* 46 (1999) 881–890.
[32] G. Revel, D.M. Alonso, J.L. Moiola, A gallery of oscillations in a resonant electric circuit: Hopf–Hopf and fold–flip interactions, *International Journal of Bifurcation and Chaos* 18 (2008) 481–494.
[33] S. Serra, C. Tablino Possio, Analytical analysis of the Gavrilov–Guckenheimer bifurcation unfolding in the case of a proportional–integral controlled CSTR, *SIAM Journal on Applied Mathematics* 59 (1999) 1716–1744.